北京理工大学
BEIJING INSTITUTE OF TECHNOLOGY

Detecting Axion Dark Matter by Artificial Magnetoelectric Materials

Chenhui XIE

2026.8.9

Axion 2026, Qingdao

Annalen Phys. 537 (2025) 12, e00202
https://doi.org/10.1002/andp.202500202

目录 | CONTENTS

1.Introduction

Axion is one of the leading candidates for dark matter (DM) .

a solution to the strong charge-parity (CP) problem in Quantum Chromodynamics (QCD) .

the extremely weak interaction with standard model (SM) particles.

In condensed matter systems, axions appear as quasiparticles in certain materials.

magnetoelectric (ME) effect : $P_i = \alpha_{ij} H_j$ or $M_i = \alpha_{ji} E_j$

α_{ij} is the magnetoelectric coupling tensor.

a magnetoelectric phenomenon in Sr2IrO4(SIO) thin films

- one based on SQUID magnetization measurements .
- another on direct ME coupling measurement system (MECMS) .

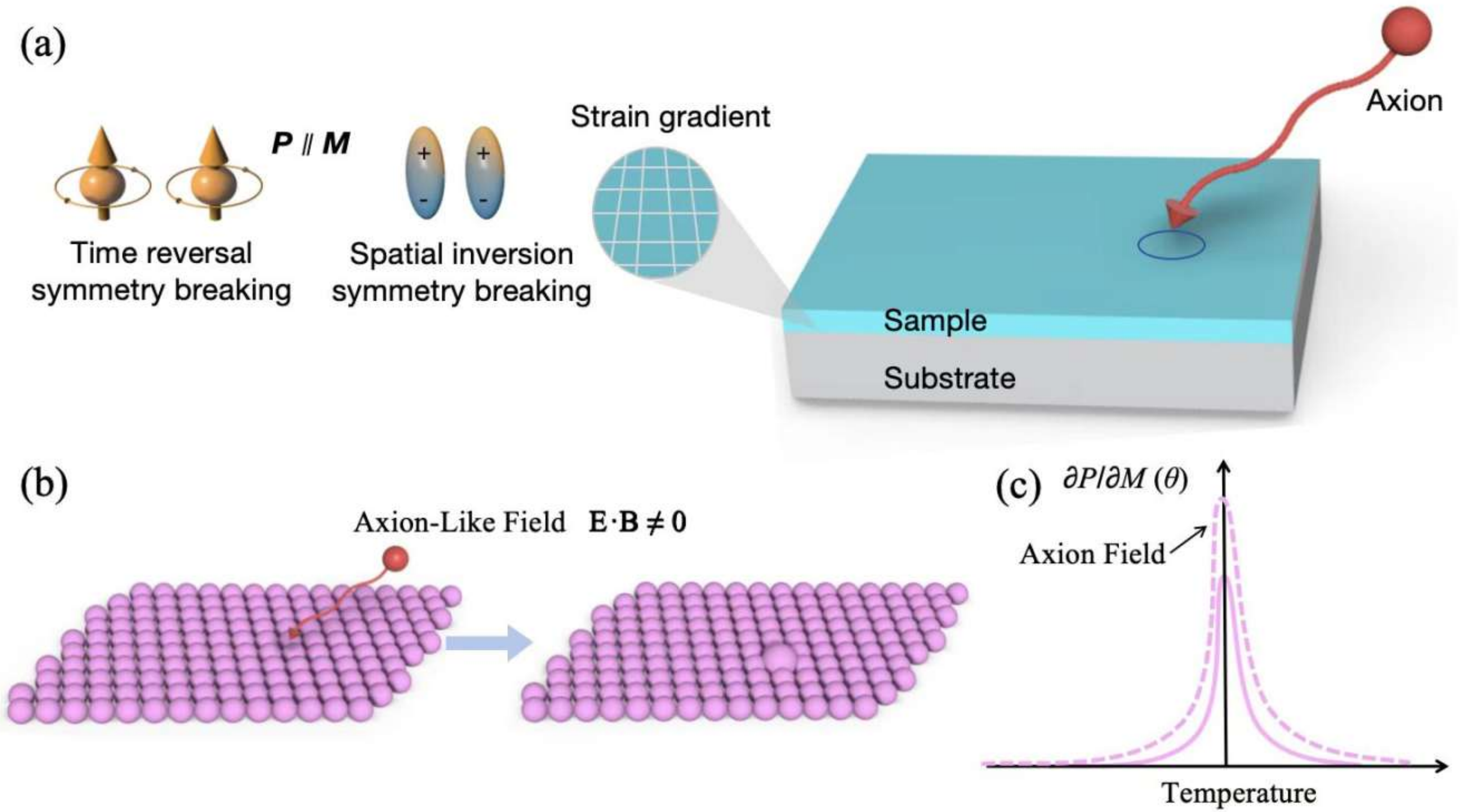

Figure 1: (a) The magnetoelectric material exhibits parallel polarization (P) and magnetization (M), corresponding to the breaking of spatial inversion symmetry and time-reversal symmetry. (b) Enlarged view within the circle of (a), where the external axion field effectively couples with the internal axion-like field in the material. (c) The magnetoelectric coupling effect is significantly enhanced after applying the external axion field.

2.Detecting Axion by Measuring Magnetization

$$\mathcal{L}_a = \frac{1}{2}(\partial_\mu a)(\partial^\mu a) - \frac{1}{2}m_a^2 a^2,$$

$$\mathcal{L}_{a\gamma\gamma} = -\frac{\theta_{a\gamma\gamma}}{4}F_{\mu\nu}\tilde{F}^{\mu\nu} = \theta_{a\gamma\gamma}\mathbf{E}\cdot\mathbf{B},$$

$$\theta_{a\gamma\gamma} \equiv a g_{a\gamma\gamma},$$

$F^{\mu\nu}$ is electromagnetic field tensor

axion-photon coupling $g_{a\gamma\gamma}$

axion field $a(t) = a_0 e^{-i\omega_a t}$.

$$\rho_{\rm DM} = \frac{1}{2}m_a^2|a_0|^2,$$

$\rho_{\rm DM}$ is the local DM density

$\rho_{\rm DM} \approx 0.4\ {\rm GeVcm}^{-3}$

Ginzburg-Landau theory

$$\mathcal{F}[\mathbf{M},\mathbf{P}] = \mu_0 \mathcal{F}_M[\mathbf{M}] + \frac{1}{\varepsilon_0}\mathcal{F}_P[\mathbf{P}] - \sqrt{\frac{\mu_0}{\varepsilon_0}}(\alpha_{ij}M^i P^j + \chi\theta\mathbf{P}\cdot\mathbf{M}),$$
$$\mathcal{F}_M[\mathbf{M}] = \alpha_M|\partial_t\mathbf{M}|^2 - \beta_M|\nabla\cdot\mathbf{M}|^2 - \gamma_M(T-T_{C_M})|\mathbf{M}|^2 - \lambda_M|\mathbf{M}|^4 + \dots,$$
$$\mathcal{F}_P[\mathbf{P}] = \alpha_P|\partial_t\mathbf{P}|^2 - \beta_P|\nabla\cdot\mathbf{P}|^2 - \gamma_P(T-T_{C_P})|\mathbf{P}|^2 - \lambda_P|\mathbf{P}|^4 + \dots,$$

α's, β's, γ's, and λ's are phenomenological coefficients

χ is a material dependent susceptibility

phase transition temperature T_{C_M} (T_{C_P})

$$\left|\frac{\delta M}{\theta_0}\right| = \frac{\chi\sqrt{4c^2P_0^2\alpha_P^2\eta_P^2\omega_a^2 + [M_0\alpha + 2cP_0(\alpha_P\omega_a^2 - m_P^2)]^2}}{\sqrt{16\omega_a^2[\alpha_M\alpha_P\omega_a^2(\eta_M+\eta_P) - \alpha_P\eta_P m_M^2 - \alpha_M\eta_M m_P^2]^2 + [\alpha^2 + 4\alpha_M\alpha_P\eta_M\eta_P\omega_a^2 - 4(\alpha_M\omega_a^2 - m_M^2)(\alpha_P\omega_a^2 - m_P^2)]^2}}.$$

$\alpha_M = 1$ meV^{-2} and $\alpha_P = 10^{-2}$ meV^{-2} $\gamma_M = 10^{-5}$ K^{-1} and $\lambda_M = 9.25$ kOe^{-2}

$\eta_M = 5$ μeV and $\eta_P = 5$ μeV damping coefficients

$\mathbf{P}_0 = \mathbf{P} - \delta\mathbf{P} = 0.6\ \mu\mathrm{C/cm}^2$ $\delta M = 1.30419 \times 10^{-8}$ emu/Vol

$\mathbf{M}_0 = \mathbf{M} - \delta\mathbf{M} = 1.16 \times 10^{-5}$ eμ/V $m_P = 4.5 \times 10^{-2}$ is the effective mass

$m_M^2 \equiv \gamma_M(T - T_{C_M}) + 6\lambda_M M_0^2$ $T_{C_M} = 20$ K

Vol= 300 nm × 2.5 mm × 2.5 mm is the size of magnetoelectric material.

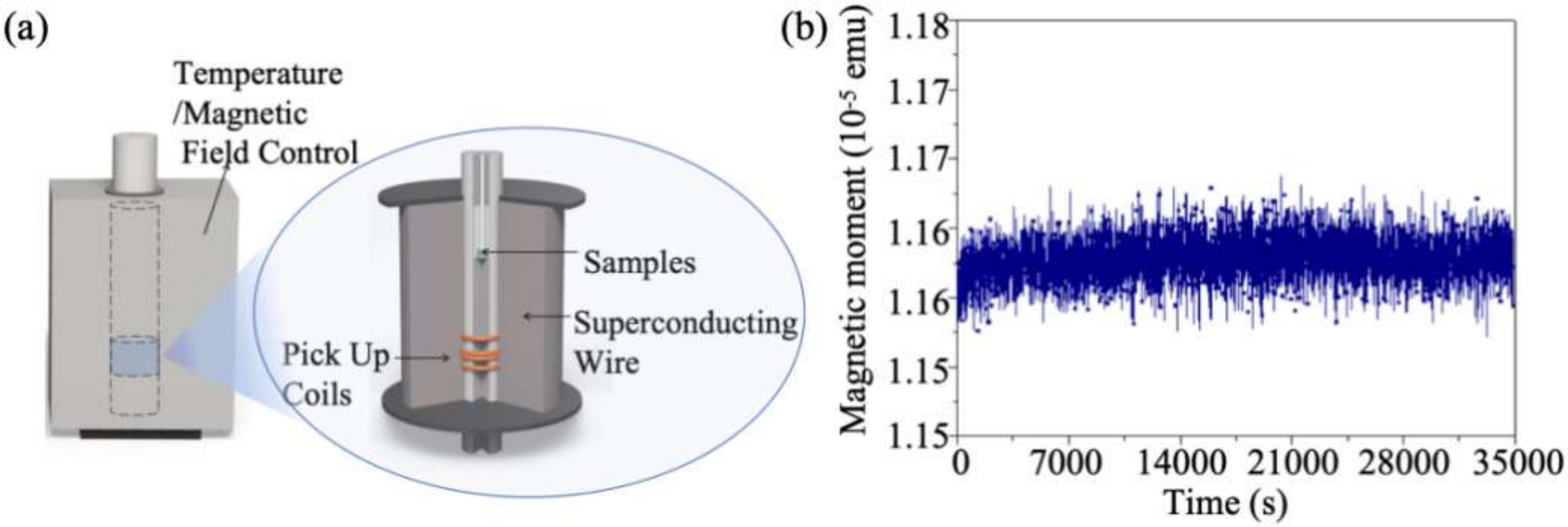

Figure 2: (a) Schematic of the SQUID measurement system, when the sample moves in the center, the magnetic flux through the coil changes, inducing an electromotive force, which in turn allows the determination of the sample's magnetic moment. (b) Time-dependent magnetization curve at 20 K.

$$\chi\theta_{ae} \equiv g_{ae} \frac{a_0 m_a \hbar}{m_e^2 c^2 g_s \alpha_E e^2} \sqrt{\frac{\varepsilon_0}{\mu_0}} \sim 7.7 \times 10^{-11} g_{ae},$$

$$\delta E_{ae}^{\mathrm{tot}} \approx L_{\mathrm{domain}}^3 \chi\theta_{ae} \sqrt{\frac{\mu_0}{\varepsilon_0}} \mathbf{P} \cdot \mathbf{M},$$

the energy change caused by axion

L_{domain} is the domain size

$\alpha_E \simeq 1/137$ is the fine structure constant

m_e is the mass of electron

$g_s \simeq 2$ is the spin g-factor of electrons

μ_0 and ϵ_0 are the permeability and permittivity the de Broglie length of the axion is larger than the material size $m_a < \frac{2\pi\hbar v_a}{l}$

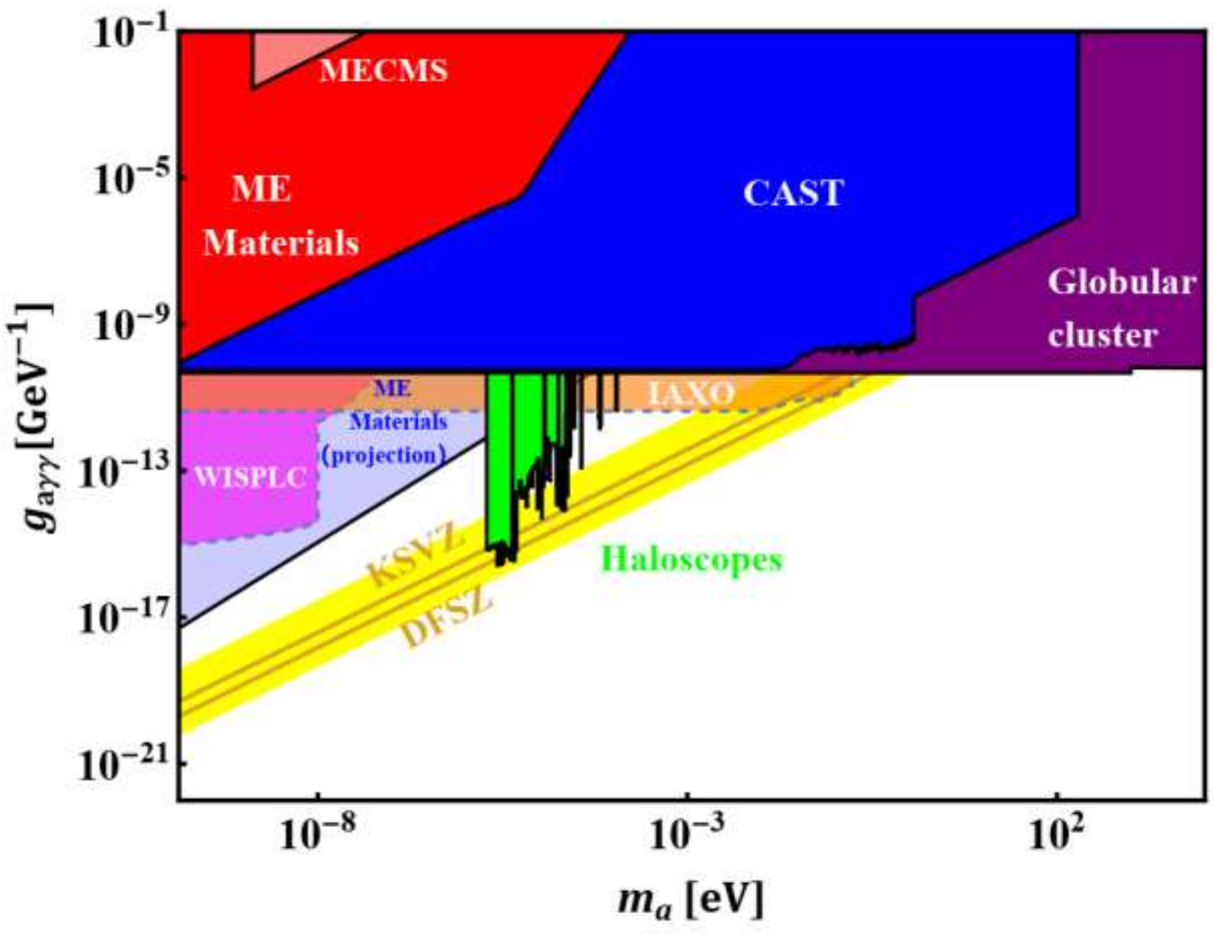

Figure 4: Constraints on the coupling factor $g_{a\gamma\gamma}$.

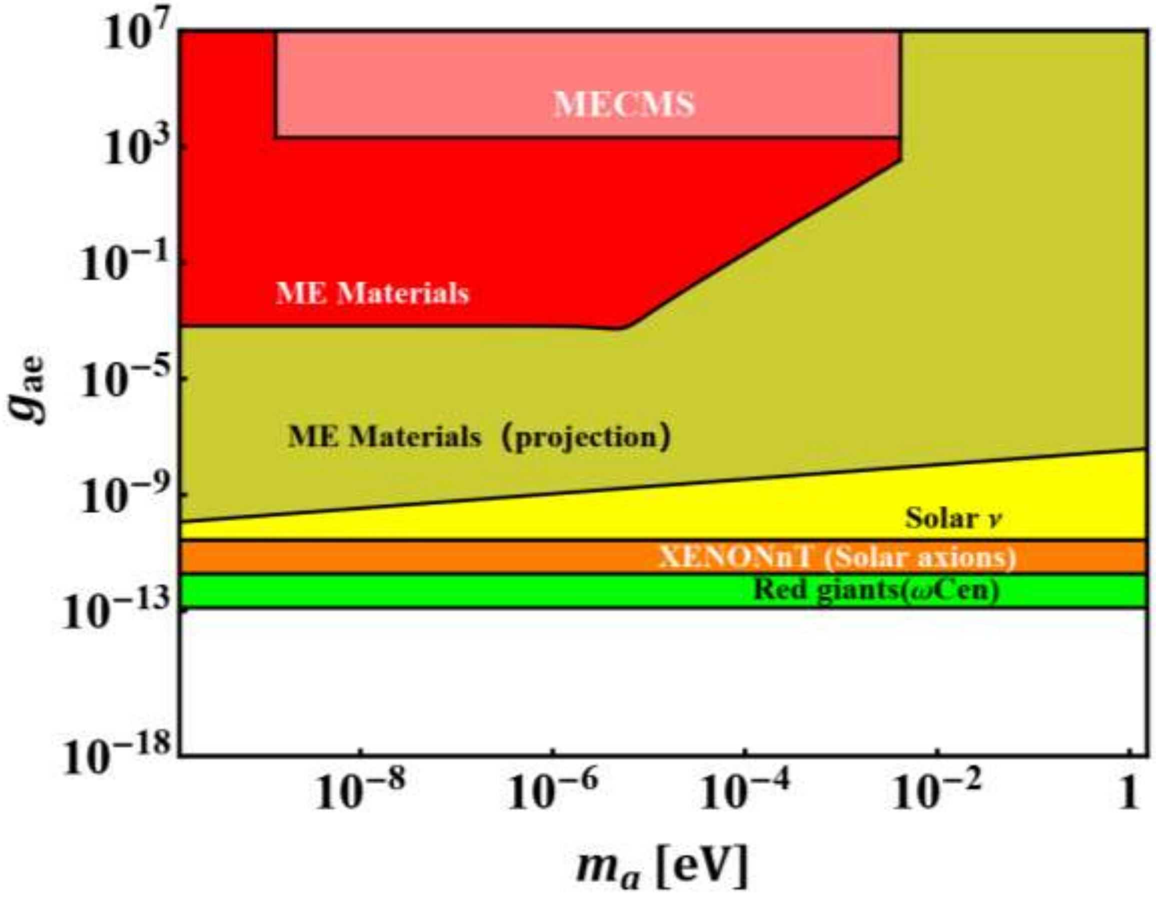

Figure 5: Constraints on the coupling factor g_{ae}.

3.the Magnetoelectric Coupling

The intrinsic magnetoelectric coupling of the material is defined by θ_{ME}

the change in magnetoelectric coupling induced by the dynamical axion field is denoted by θ.

the total magnetoelectric coupling of the material $\theta_{tot} = \theta_{\mathrm{ME}} + \theta.$

linear magnetoelectric coupling coefficient $$\alpha_{ij} = \left.\frac{\partial P_i}{\partial H_j}\right|_{\mathbf{E}=0}.$$

$$\theta_{\mathrm{ME}} = \frac{4\pi^2 \hbar c \alpha}{e^2}.$$

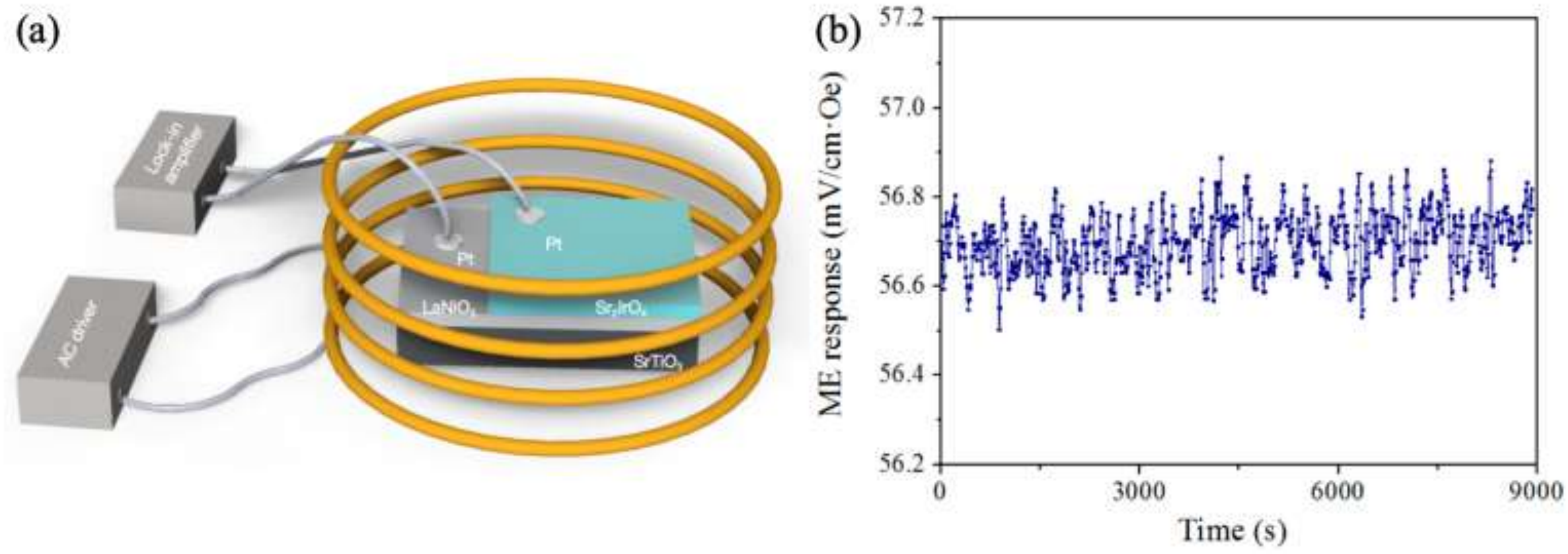

FIG. 3. (a) Schematic of the magnetoelectric coupling measurement system. Alternating current is applied to generate an alternating magnetic field, and the alternating electrical signal induced in the sample is detected by a lock-in amplifier.(b) Time-dependent magnetoelectric response curve.

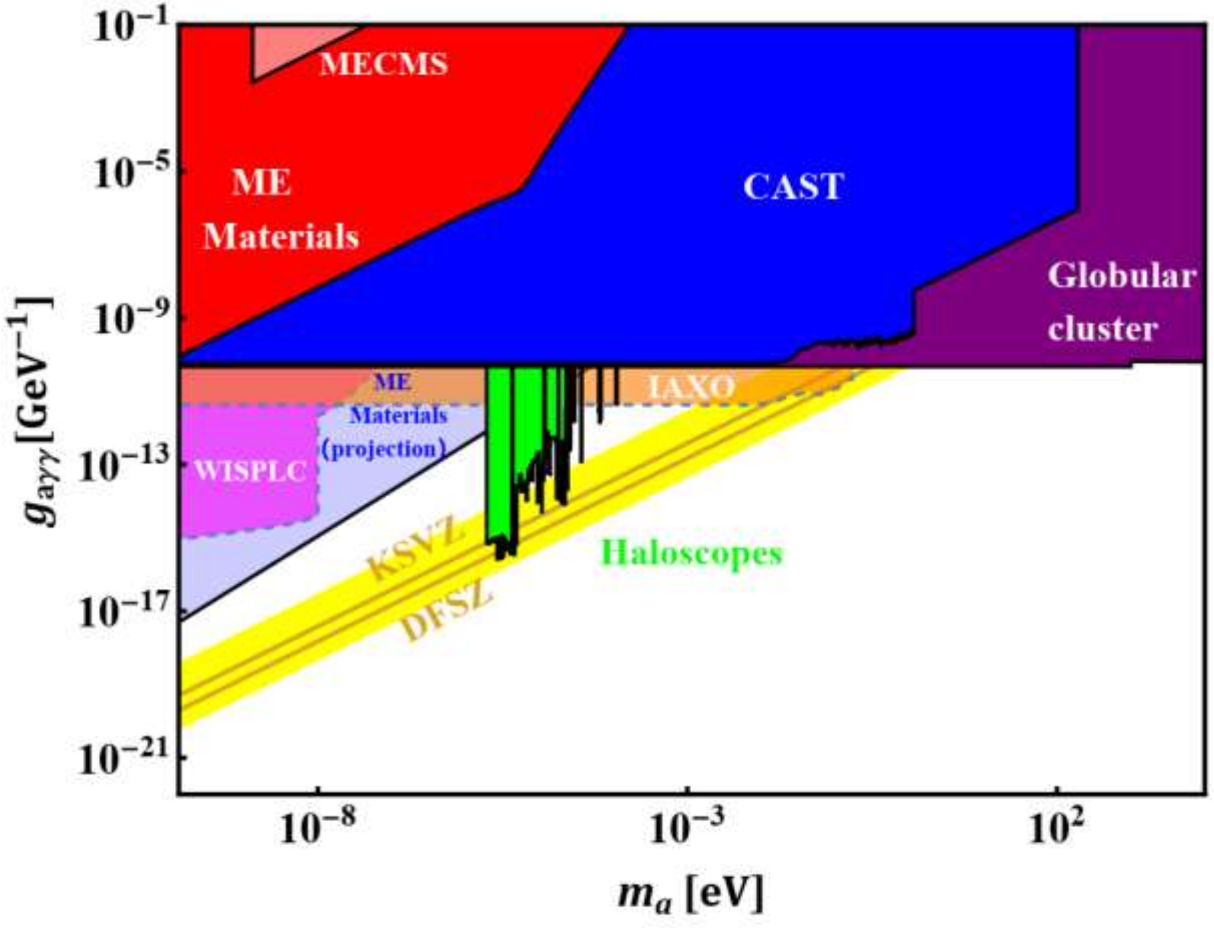

Figure 4: Constraints on the coupling factor $g_{a\gamma\gamma}$.

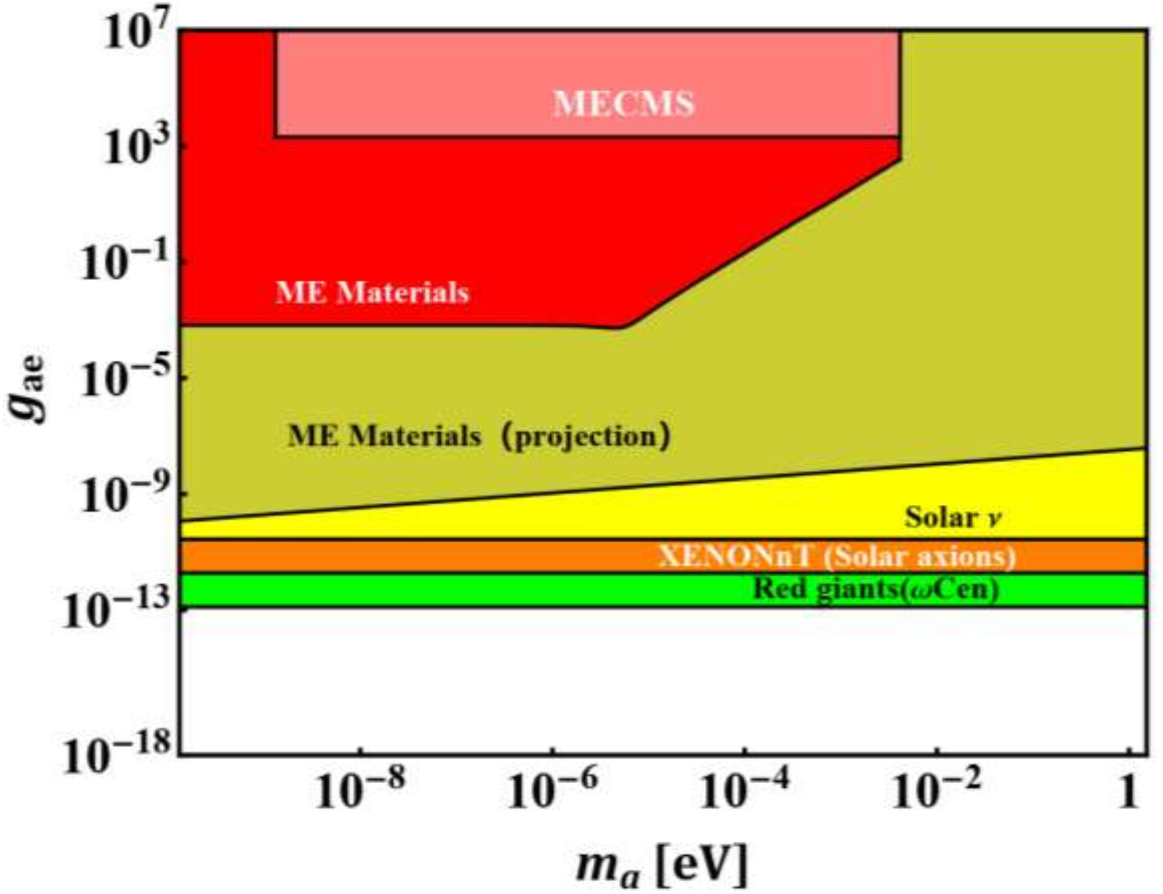

Figure 5: Constraints on the coupling factor g_{ae}.

4.Discussion and Future Projection

The experiment sensitivity for the first method to detect axion

signal-to-noise ratio (SNR) $\mathrm{SNR} \sim \frac{V}{\gamma T} \frac{|P_0|^2}{\Delta\omega_a \alpha_M} (\chi\theta)^2 \sqrt{\frac{\Delta\omega_a}{\Delta\omega_{\mathrm{meas}}}},$

V is the size of the projected Magnetoelectric Material sample $0.1 \times 0.1 \times 0.01\ \mathrm{m}^3.$

measurement time $t_{\mathrm{meas}} = 1$ year.

$\Delta\omega_{\mathrm{meas}} \sim t_{\mathrm{meas}}^{-1}$ the measurement bandwidth

$\Delta\omega_a \sim \frac{1}{2}\omega_a v_a^2$ is the width of the axion signal

$\gamma \sim 10^{-6}$ eV is the width of the magnetic resonance

SNR=3

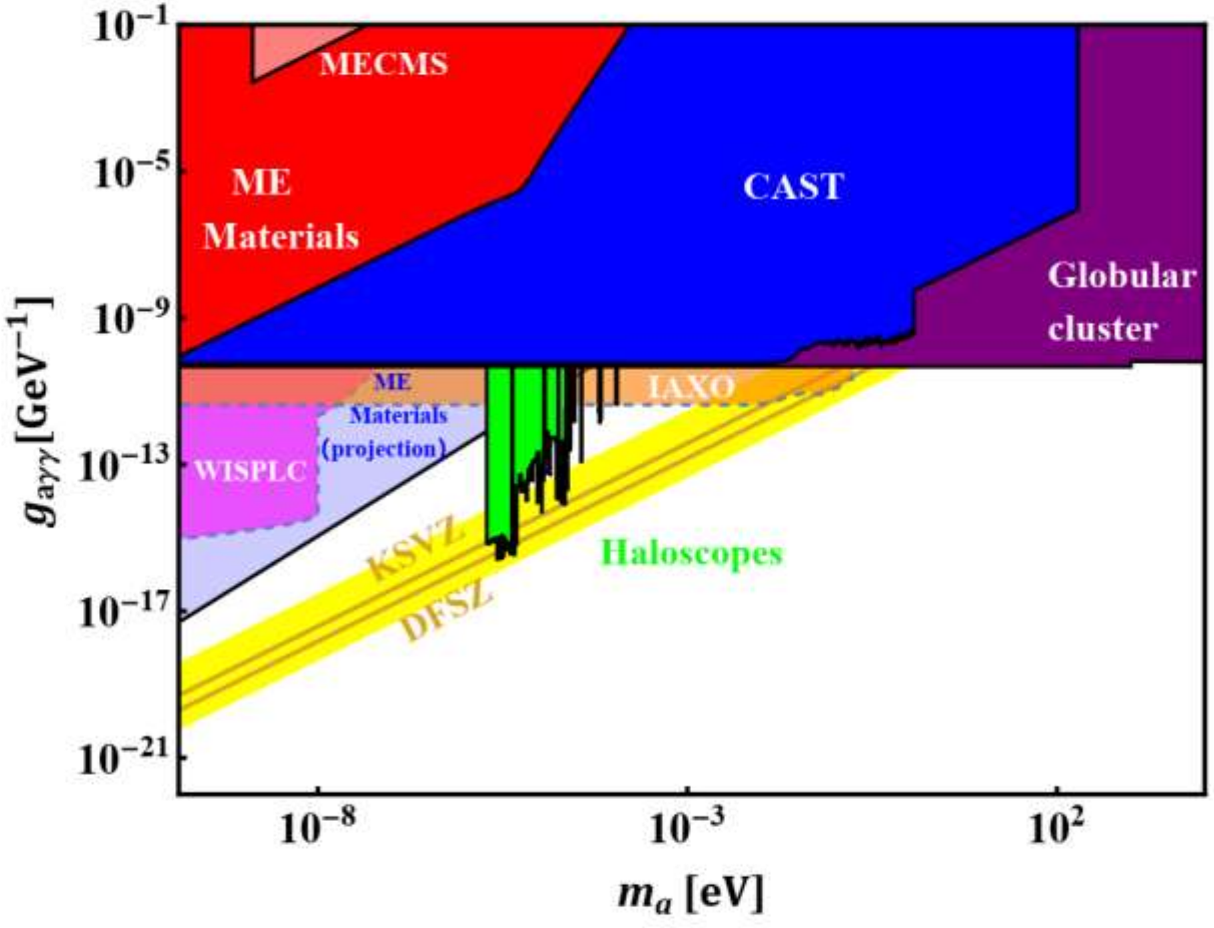

Figure 4: Constraints on the coupling factor $g_{a\gamma\gamma}$.

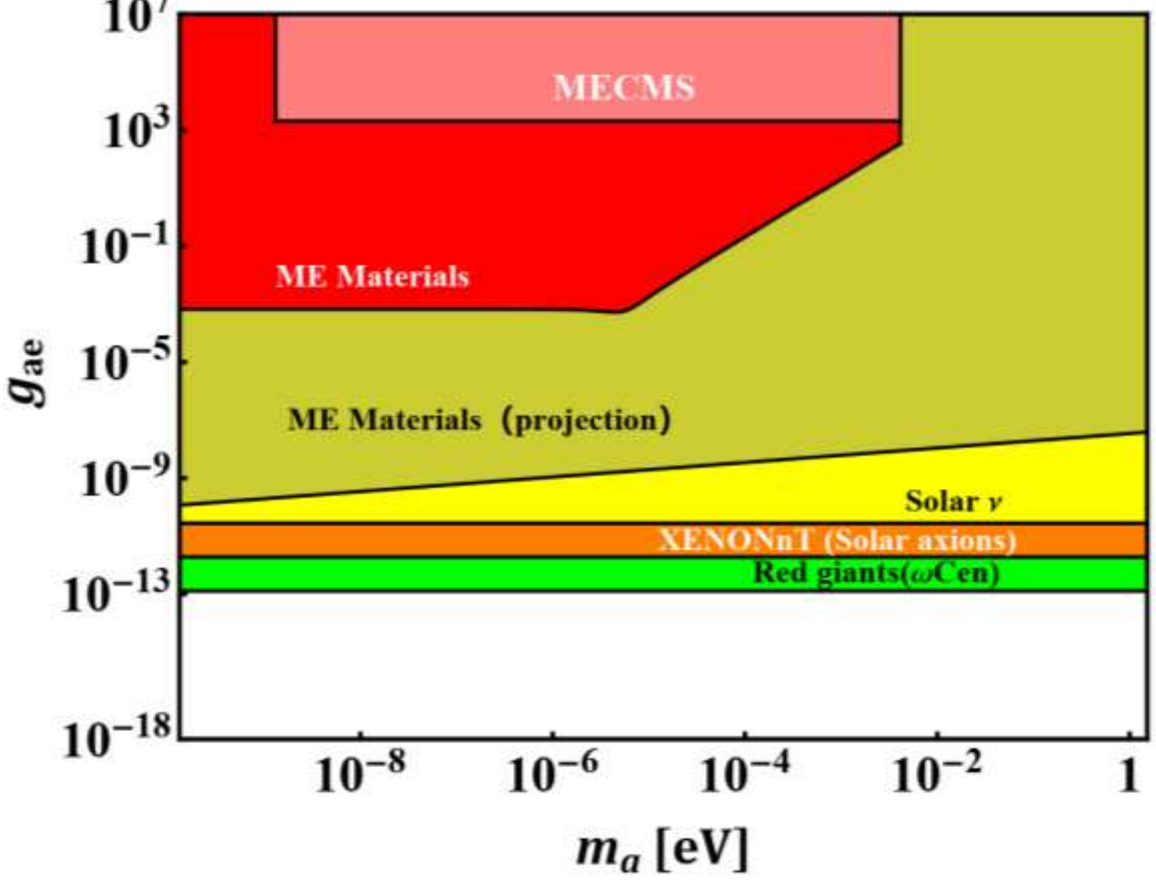

Figure 5: Constraints on the coupling factor g_{ae}.

5.Conclusion and Outlook

This study presents a novel approach for detecting axion dark matter using magnetoelectric (ME) materials, combining the strengths of SQUID-based magnetization measurements and direct magnetoelectric coupling experiments.

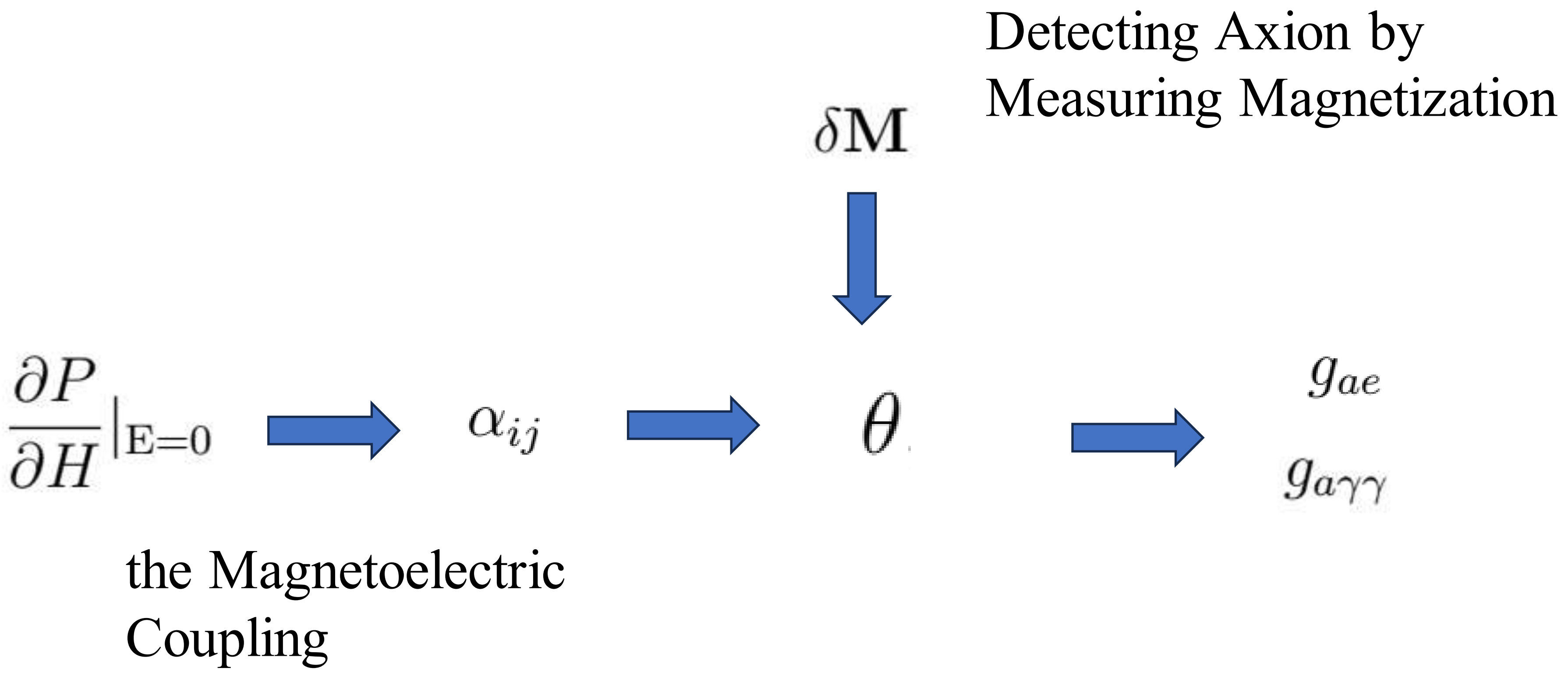
Detecting Axion by
Measuring Magnetization
$\delta\mathbf{M}$
$\frac{\partial P}{\partial H}|_{\mathrm{E}=0}$
α_{ij}
θ
g_{ae}
$g_{a\gamma\gamma}$
the Magnetoelectric
Coupling

References:

[1] R. D. Peccei, H. R. Quinn, CP Conservation in the Presence of Instantons, Phys. Rev. Lett. 1977, 38 1440.

[2] R. D. Peccei, H. R. Quinn, Constraints Imposed by CP Conservation in the Presence of Instantons, Phys. Rev. D 1977, 16 1791.

[3] S. Weinberg, A New Light Boson?, Phys. Rev. Lett. 1978, 40 223.

[4] F. Wilczek, Problem of Strong *P* and *T* Invariance in the Presence of Instantons, Phys. Rev. Lett. 1978, 40 279.

[5] A. J. Millar, G. G. Raffelt, J. Redondo, F. D. Steffen, Dielectric Haloscopes to Search for Axion Dark Matter: Theoretical Foundations, JCAP 2017, 01 061.

[6] A. Mitridate, T. Trickle, Z. Zhang, K. M. Zurek, Detectability of Axion Dark Matter with Phonon Polaritons and Magnons, Phys. Rev. D 2020, 102, 9 095005

[7] S. Chigusa, T. Moroi, K. Nakayama, Detecting light boson dark matter through conversion into a magnon, Phys. Rev. D 2020, 101 096013.

[8] D. Budker, P. W. Graham, M. Ledbetter, S. Rajendran, A. Sushkov, Proposal for a Cosmic Axion Spin Precession Experiment (CASPEr), Phys. Rev. X 2014, 4, 2 021030.

[9] H. Ooguri, M. Oshikawa, Instability in Magnetic Materials with a Dynamical Axion Field, Phys. Rev. Lett. 2012, 108 161803.

[10] J. Lee, K. Murai, F. Takahashi, W. Yin, More is Different: Multi-Axion Dynamics Changes Topological Defect Evolution, arXiv preprint arXiv:2409.09749 2024.